




Article

Grain Size Engineering and Tuning of Magnetic Properties in Ultra-Thin NiMnGa Glass-Coated Microwires: Insights from Annealing Effects

Mohamed Salaheldeen ^{1,2,3,4,*} , Valentina Zhukova ^{1,2,4} , Julian Gonzalez ¹ and Arcady Zhukov ^{1,2,4,5,*} 

¹ Department of Polymers and Advanced Materials, Faculty of Chemistry, University of the Basque Country, UPV/EHU, 20018 San Sebastián, Spain; valentina.zhukova@ehu.eus (V.Z.); julianmaria.gonzalez@ehu.eus (J.G.)

² Department of Applied Physics I, EIG, University of the Basque Country, UPV/EHU, 20018 San Sebastián, Spain

³ Physics Department, Faculty of Science, Sohag University, Sohag 82524, Egypt

⁴ EHU Quantum Center, University of the Basque Country, UPV/EHU, 20018 San Sebastián, Spain

⁵ IKERBASQUE, Basque Foundation for Science, 48011 Bilbao, Spain

* Correspondence: mohamed.salaheldeenmohamed@ehu.eus (M.S.); arkadi.joukov@ehu.es (A.Z.)

Abstract: We studied the influence of annealing on the magnetic properties and microstructure of ultrathin (metallic nucleus diameter $\approx 5 \mu\text{m}$, total diameter $\approx 19 \mu\text{m}$) Heusler-type NiMnGa glass-coated microwires prepared using the Taylor–Ulitsky method. The as-prepared NiMnGa microwires exhibit unexpectedly strong magnetic anisotropy, characterized by a coercivity exceeding 3 kOe at room temperature. Furthermore, their Curie temperature (T_c) lies above room temperature. Additionally, a spontaneous exchange bias of approximately 120 Oe is observed in the as-prepared sample at 100 K. Annealing the microwires leads to a decrease in coercivity, spontaneous exchange bias, and T_c values. Notably, the annealing process shifts the T_c of the samples closer to room temperature, making them more suitable for magnetic solid-state refrigeration applications. Moreover, the hysteresis observed in the temperature dependence of magnetization for the samples annealed for 1 h and 2 h, along with the magnetic softening observed at around 260 K, is attributed to a first-order phase transformation. The observed changes are discussed in the context of internal stress relaxation after annealing, the nanocrystalline structure of both the as-prepared and annealed samples, the recrystallization process, and the magnetic ordering of phases identified in the as-prepared sample and those appearing during recrystallization. The glass coating on microwires offers benefits like better flexibility and resistance to damage and corrosion. However, it is important to recognize that this coating can substantially alter the microwires' magnetic characteristics. Consequently, precise control over the annealing process is vital to obtain the specific martensitic transformation needed.

Keywords: Heusler alloys; glass-coated microwires; nanocrystalline; annealing; grain size; martensitic transformation



check for updates

Academic Editors: Marzena Lachowicz and Erdem Karakulak

Received: 12 May 2025

Revised: 11 June 2025

Accepted: 14 June 2025

Published: 16 June 2025

Citation: Salaheldeen, M.; Zhukova, V.; Gonzalez, J.; Zhukov, A. Grain Size Engineering and Tuning of Magnetic Properties in Ultra-Thin NiMnGa Glass-Coated Microwires: Insights from Annealing Effects. *Crystals* **2025**, *15*, 565. <https://doi.org/10.3390/cryst15060565>

Copyright: © 2025 by the authors. Licensee MDPI, Basel, Switzerland. This article is an open access article distributed under the terms and conditions of the Creative Commons Attribution (CC BY) license (<https://creativecommons.org/licenses/by/4.0/>).

1. Introduction

The study of magnetic materials that undergo thermoelastic martensitic phase transformations (TMPTs) has garnered considerable interest recently due to their distinctive and advantageous characteristics [1–6]. These materials display impressive attributes such as both elastocaloric and magnetocaloric (EMC) effects [1,2,4,7–12], shape memory (SM) [13–18], significant superelasticity (GS) [14–26], magnetic field-induced strain (MFIS) [1,2,12,16–22],

and magnetoresistance (MR) [17,20]. Such extraordinary properties pave the way for a wide range of potential applications across numerous domains [20,21,23–28].

The notable attention given to Ni–Mn–Ga Heusler alloys stems from their unique ability to undergo a reversible, diffusionless phase transformation. This process involves a structural change from a high-symmetry cubic austenite phase to a lower-symmetry martensite phase. As a result of this notable characteristic, Ni–Mn–Ga alloys possess several useful functional capabilities, such as the magnetic shape memory effect (MSME), strain induced by a magnetic field (MFIS), and the magnetocaloric effect (MCE) [12,21,29]. Conventional shape memory alloys (SMAs) demonstrate remarkable reversibility in their shape changes between austenite and martensite phases [12,29–34]. Triggered by variations in temperature or stress, this property makes them ideal candidates for actuators, sensors, and energy transducers requiring both high-frequency responses and significant recoverable strains. The development of smaller SMA-based devices has fueled the requirement for SMA materials in miniature shapes like particles, wires, ribbons, films, and microstructures. However, Ni–Mn–Ga alloys, which typically belong to the class of intermetallic compounds, suffer from inherent brittleness [32–40]. A major drawback of this characteristic is the difficulty that it creates for traditional fabrication processes like cold drawing or forging. While single crystals display better ductility, their lengthy and segregation-prone production method ultimately leads to a reduction in their performance capabilities [16,18,20,21,25,26].

The Taylor–Ulitsky technique for producing Ni–Mn–Ga glass-coated microwires presents a potential solution to the challenges associated with Ni–Mn–Ga fabrication [7,19,39–41]. This technique offers two key advantages: firstly, it facilitates the creation of long glass-coated microwires, reaching lengths up to 10 km with diameters ranging from 0.1 to 100 μm [19,40–46]. Secondly, the glass coating enhances the mechanical properties of the microwire brittle nucleus with a crystalline structure [47]. Moreover, these microwires are especially well-suited for microactuator applications due to their cylindrical form, which allows them to perform as thin wires. Recent studies underscore the versatility of this technique, having successfully produced glass-coated microwires with a range of chemical compositions and crystal structures [40–51].

Initial endeavors to synthesize Heusler-type glass-coated microwires with Ni–Mn–Ga compositions began approximately a decade ago [7,40,45]. Nevertheless, these early efforts encountered obstacles. The evaporation of manganese during the manufacturing process led to deviations from the desired chemical composition, and inherent internal stresses prevented the anticipated martensitic transformation (MT) from occurring [7,40]. These internal stresses in glass-coated microwires are attributable to several elements, including the continuous drawing of the wire, the rapid solidification of the metallic core, and the difference in thermal expansion coefficients (CTE) between the glass coating and the metallic alloy [48,51].

Recent research has explored new approaches to address these limitations. For instance, martensitic transformation (MT) was detected in uncoated, thick Ni–Mn–Ga microwires following an annealing treatment [43]. In another study, X. Zhang et al. achieved MT in Ni–Mn–In–Co microwires, but only after stripping the glass coating [52]. Importantly, MT has so far only been observed either in uncoated microwires—which undermines a major advantage of the Taylor–Ulitsky method—or in meticulously annealed NiMnGa-based glass-coated microwires [19,53,54]. Thus, determining the ideal fabrication parameters is essential to induce MT and fully harness the multifunctional properties of Heusler-type microwires.

This research examines the martensitic transformation (MT) in ultra-thin Ni–Mn–Ga glass-coated microwires (diameter < 6 μm) produced via the Taylor–Ulitsky method. Notably, post-annealing triggers a distinct MT at low temperatures and under weak mag-

netic fields—a surprising result given the substantial nickel excess and prior evidence of high-temperature MT in bulk alloys with similar compositions. Additionally, the study analyzes how annealing temperature, duration, and the retention of the glass coating affect the microwires' magnetic properties and Curie temperature.

2. Materials and Methods

2.1. Fabrication of Bulk NiMnGa Form

This research focuses on manufacturing slender, glass-coated microwires utilizing the Ni–Mn–Ga alloy system. The fabrication process essentially comprises two primary phases: initially, creating a bulk Ni–Mn–Ga alloy ingot, followed by transforming this ingot into microwires (as illustrated in Figure 1a,b). The initial phase entails the careful production of a Ni₅₀Mn₂₅Ga₂₅ bulk alloy through arc melting. The synthesis process starts with high-purity (99.99 wt.%) elemental powders of Ni, Mn, and Ga. To obtain the desired Ni₅₀Mn₂₅Ga₂₅ composition, the powders are precisely weighed to maintain stoichiometric accuracy. The measured mixture is then loaded into a high-temperature-resistant graphite crucible, which is placed in an electric arc furnace chamber under a vacuum and argon atmosphere. An electric arc is generated between the electrode and crucible, producing extreme localized heat that melts the powder blend. To ensure complete liquefaction and homogenous mixing of all elements, the melting process is meticulously controlled. Following the completion of melting, the electric arc is extinguished, and the molten metal is allowed to cool progressively within the controlled environment. A uniform and homogenous Ni₅₀Mn₂₅Ga₂₅ bulk alloy ingot is promoted via this controlled cooling. Additionally, the ingot can be put through several remelting cycles to further improve its microstructural homogeneity and raise its overall quality. This stage involves multiple (typically five) melting and homogenization cycles. Repeated remelting enhances the compositional uniformity and helps refine the alloy's grain structure. Following solidification, the Ni–Mn–Ga bulk alloy ingot is characterized using various analytical techniques to evaluate its structural and compositional properties. This quality control step is essential to verify the material's suitability for subsequent microwire production.

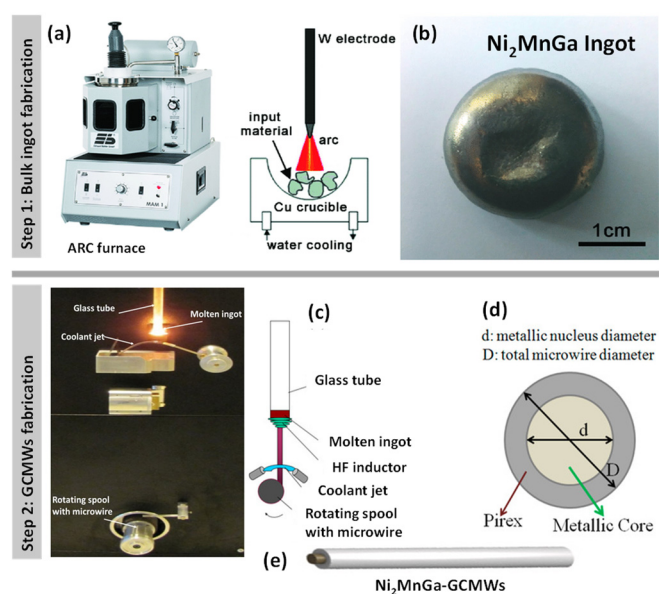


Figure 1. Illustration of the experimental facility and key steps involved in fabricating thin Ni₂MnGa-glass-coated microwires. Panels (a,b) show the ARC melting furnace and the resulting bulk alloy ingot. Panel (c) depicts the Taylor–Ulitovsky method used for producing the glass-coated microwires, while panels (d,e) provide schematic illustrations of the Ni₂MnGa-based glass-coated microwires themselves.

2.2. Preparation of NiMnGa Glass-Coated Microwires

Microwires covered with Duran glass coating were fabricated using the Taylor–Ulitsky technique described in detail elsewhere [51,55–59] (see Figure 1c–e). The Taylor–Ulitsky technique involves inserting the master alloy into a glass (e.g., Duran) tube, which is then locally heated to soften the glass and melt the alloy. Subsequently, a glass capillary containing the molten metallic nucleus is drawn, resulting in a composite microwire with a metallic core and a glass coating. The microwires possess an overall diameter (D) of 19.7 μm and a metallic core diameter (d) measuring 5.2 μm . Energy-dispersive X-ray (EDX) analysis validated a chemical composition of $\text{Ni}_{54}\text{Mn}_{22}\text{Ga}_{24}$ (with an error margin of 0.5%). This composition deviates from the intended stoichiometry [60], primarily due to the evaporation of manganese during the initial ingot melting and subsequent microwire manufacturing stages, including casting and drawing.

The as-prepared glass-coated microwires were encapsulated between two ceramic plates and subjected to an annealing at 973 K for varying durations (1 h, 2 h, and 4 h) within a vacuum environment (pressure $P = 2 \times 10^{-4}$ Pa). The heating rate employed was 10 K/min, followed by furnace cooling. Following the annealing process, EDX analysis was performed to assess how the annealing time might affect the chemical composition. The analysis revealed a change in composition for the microwires annealed at 973 K: $\text{Ni}_{54}\text{Mn}_{22}\text{Ga}_{24}$ for 1 h, $\text{Ni}_{53}\text{Mn}_{21}\text{Ga}_{26}$ for 2 h, and $\text{Ni}_{55}\text{Mn}_{20.5}\text{Ga}_{24.5}$ for 4 h.

2.3. Structural and Magnetic Characterization Methods

X-ray diffraction (XRD) measurements were performed at ambient temperature utilizing a Bragg–Brentano geometry diffractometer (Bruker D8 Discovery, Bruker AXS, Karlsruhe, Germany) with monochromatic $\text{Cu K}\alpha$ radiation ($\lambda = 1.5406$ Å). A bundle of parallel microwires was carefully arranged and fixed onto a sample holder. This assembly, rather than a coil, was then placed under the X-ray beam in the Bragg–Brentano geometry diffractometer. Scans were acquired in a θ – 2θ configuration with an angular step size of 0.02° over the 2θ range of 0 – 80° . Magnetic characterization was conducted employing a Quantum Design Physical Property Measurement System (PPMS) integrated with a vibrating sample magnetometer (VSM). Temperature-dependent magnetization measurements were executed under an axial magnetic field of 50 Oe across the temperature interval 5–400 K. The measurement protocol comprised the following sequence:

- Zero-field cooling (ZFC): The sample was cooled from 400 K (paramagnetic regime) in the absence of an applied field.
- Field-cooled (FC) measurement: Upon reaching 5 K, a static magnetic field of 50 Oe was applied, and magnetization data were acquired during subsequent heating to 350 K.
- Field-heated (FH) measurement: Maintaining the applied field, data collection continued during cooling and the subsequent reheating cycles.

All the temperature sweeps were performed at a constant rate of 2 K min^{-1} .

Isothermal magnetic hysteresis measurements were additionally performed at discrete temperatures between 5 and 300 K, with the applied magnetic field oriented parallel to the microwire axis and swept to a maximum intensity of 30 kOe. For improved comparison of the results, all magnetic data are normalized, presented as M/M_{sat} or $M/M_{5\text{K}}$. Here, M_{sat} denotes the magnetic moment measured at the saturation field, while $M_{5\text{K}}$ refers to the magnetic moment recorded at 5 K. The Curie temperature (T_c) was determined by finding the minimum point of the first derivative of the magnetic moment versus temperature curves.

3. Results

3.1. Structure Characterizations

X-ray diffraction (XRD) patterns of as-prepared glass-coated NiMnGa microwires annealed at 973 K for various durations were obtained at room temperature. These XRD patterns are presented in Figure 2. A prominent broad peak is observed in the low-angle region of the XRD pattern at approximately $2\theta \approx 22^\circ$. This feature can be attributed to the presence of the amorphous glass coating surrounding the NiMnGa nucleus. Similar observations and interpretations have been reported elsewhere in the literature for microwires [30,59,61–64]. In all the wires, the austenitic cubic phase at room temperature with an Fm-3m space group and L2₁ ordered structure was confirmed from the XRD patterns. This agrees with our previous investigation in NiMnGa-based glass-coated microwires with a larger metallic nuclei diameter [61]. Notably, there is the presence of a well-defined peak corresponding to the (220) reflection at around $2\theta \approx 44^\circ$ for the as-prepared sample. This peak shifted toward the low angle by increasing the duration of the annealed temperature (see the right inset of Figure 2). Such monotonic shifting of the (220) peaks is first reported for the ultra-thin NiMnGa-glass-coated microwires. For the as-prepared sample, three main peaks with reflections (220), (311) and (400) are observed at $2\theta \approx 44^\circ$, 48° , and 64° , respectively. For the sample annealed at 973 K for 1 h, an additional peak at $2\theta \approx 24^\circ$ with reflection (111) is observed. For samples annealed for 2 h, similar peaks and reflections are observed for the as-prepared sample, while in the sample annealed for 4 h, a new peak is observed at $2\theta \approx 36^\circ$ with reflection (200), and the peak at $2\theta \approx 64^\circ$ disappears. This behavior can suggest a redistribution of elements (Ni, Mn, Ga) on the crystallographic sites within the L2₁ structure, potentially affecting the degree of atomic order. Annealing can promote atomic diffusion, leading to such reordering or even slight changes in the site occupancy factors. Also, the observed monotonic shift of the (220) reflection towards lower 2θ angles with increasing annealing duration (as seen in the inset of Figure 2) indicates an expansion of the L2₁ austenitic unit cell. The origin of this lattice expansion upon annealing is likely multifactorial. Firstly, changes in the precise chemical composition of the metallic nucleus during annealing can significantly influence the lattice parameters. Our EDX analysis (Section 2.2) revealed alterations in stoichiometry with annealing time; for example, the composition changed from Ni₅₄Mn₂₂Ga₂₄ for the 1 h, Ni₅₃Mn₂₁Ga₂₆ for the 2 h, and Ni₅₅Mn_{20.5}Ga_{24.5} for the 4 h annealed samples. Such variations, particularly in the relative amounts of Ni, Mn, and Ga, which possess different atomic radii, can lead to changes in the average unit cell volume. Secondly, the annealing process facilitates the relaxation of internal stresses. These stresses are inherent in glass-coated microwires due to the rapid solidification and the differential thermal expansion coefficients between the metallic core and the glass coating. The reduction in compressive internal stresses acting on the metallic nucleus would naturally allow for an expansion of its crystal lattice. Therefore, the observed lattice expansion is attributed to a combination of these compositional adjustments and internal stress relaxation occurring during the annealing treatment. Additionally, a notable reduction in the diffraction intensity is seen as compared to the as-prepared sample. Further increasing the annealing time resulted in a notable reduction in the diffraction intensity being observed where the sample with an annealing time of 4 h showed the lowest diffraction intensity. These reductions in the diffraction intensity are due to the changing in the microstructure of the sample induced by the annealing process. This changing in the XRD diffractions reveals the strong effect of the annealing time, t_{ann} , and temperature, T_{ann} , on the microstructure of NiMnGa-based glass-coated microwires. The XRD results for studied ultra-thin NiMnGa-based glass-coated microwire ($d \approx 5.2 \mu\text{m}$) differ from those observed in NiMnGa-glass-coated microwires with $d > 6 \mu\text{m}$. Indeed, for the NiMnGa-glass-coated microwires with thicker d or high geometric aspect ratios, the

different secondary phase and different degree of ordered and disordered microstructure are observed after annealing.

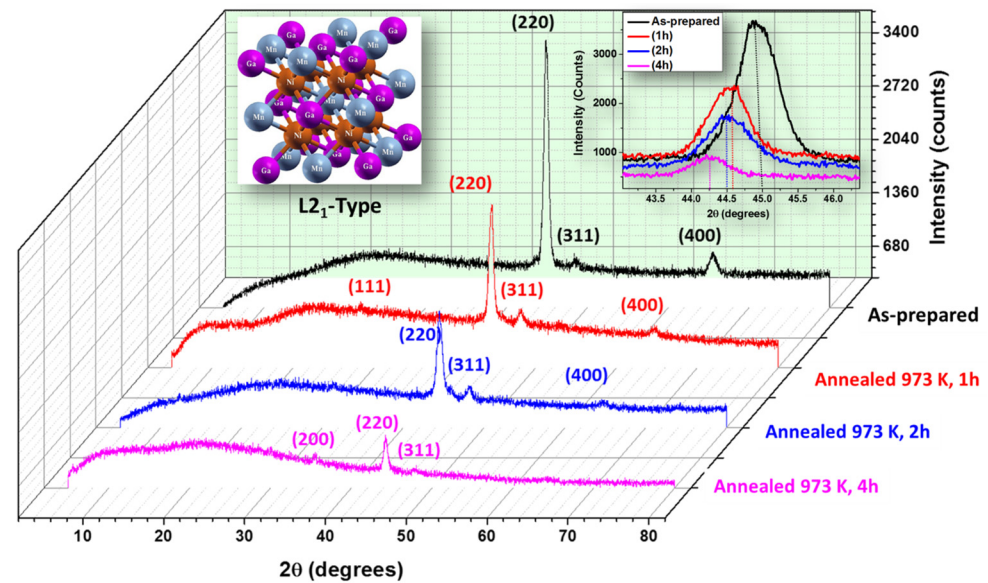


Figure 2. Room temperature XRD patterns are presented for samples in their as-prepared state and after annealing at 973 K and different annealing times (1 h, 2 h, and 4 h) of thin NiMnGa-based glass-coated microwire. The right inset illustrates the monotonic main peak displacement toward the low angle with increasing time of annealing, and the left inset illustrates the crystal structure of L₂₁-type phase for standard Ni–Mn–Ga Heusler alloy.

The average crystallite size (D_g) of the samples can be estimated using the Debye–Scherrer equation relating the broadening of a diffraction peak to the size of the crystallites causing the diffraction and given as:

$$D_g = K\lambda / (B \cos(\theta)) \quad (1)$$

K : Dimensionless Scherrer shape factor, typically taken as 0.9 for spherical crystals;

λ : X-ray wavelength (0.154 nm for Cu $K\alpha_1$ radiation);

B : Full width at the half maximum (FWHM) of the diffraction peak (in radians);

θ : Bragg diffraction angle (corresponding to $2\theta \approx 22^\circ$ for the measured peak).

The overall diffraction pattern represents the combined contributions from both the crystalline and amorphous phases within the NiMnGa glass-coated microwire samples. The relative amount of crystalline material, C_{pc} , can be quantified by analyzing the integrated intensities of the corresponding peaks, I_c , determined from the following equation [65,66]:

$$C_{pc} = \frac{I_c}{I_c + I_a \left(0.1 + e^{-\frac{D_g}{25}}\right)} \quad (2)$$

Here, I_c represents the integrated intensity of the crystalline component, I_a is the integrated intensity of the amorphous peak, and 25 is a constant expressed in nm [67]. The crystalline phase content, denoted as C_{pc} , for the as-prepared and annealed NiMnGa glass-coated microwire samples can be determined by evaluating the total area under the relevant diffraction features (encompassing both crystalline and amorphous contributions).

As presented in Figure 3, a significant increase in the D_g from 13 nm for the as-prepared sample reached the maximum ($D_g = 42$ nm) for the annealed sample for $t_{ann} = 4$ h. For C_{pc} estimation, the as-prepared sample shows a quite high C_{pc} of about 85%. This value increases towards 92% and 93% for the samples annealed for $t_{ann} = 1$ h and $t_{ann} = 2$ h, respectively. Then, a sharp drop to 86% in the C_{pc} value for the annealed sample at 4 h is observed. It is commonly assumed that the annealing typically promotes grain growth

in NiMnGa alloys. Typically, after annealing the coarsening of existing grains, a decrease in the number of grain boundaries is reported. This results in an increase in the average grain size. In addition, this increasing in D_g value is due to enhanced atomic diffusion at higher temperatures where the atoms achieve higher mobility to become agglomerated with each other leading to larger crystallite sizes [60]. Moreover, the recrystallization of the amorphous phase into the bcc phase should be associated with the increase in D_g by increasing the annealing time [68–70].

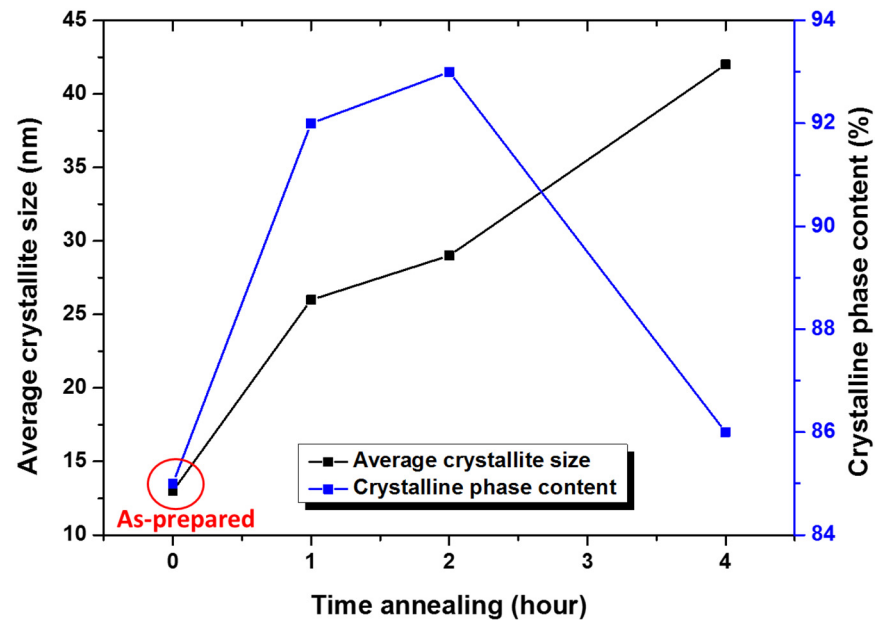


Figure 3. The average crystallite grain size and the crystalline phase content as a function of the annealing time of NiMnGa-based glass-coated microwires.

However, a decrease in the D_g upon annealing has been previously reported in several nanocrystalline materials [71]. As previously discussed, such unusual D_g decrease can be explained either via the devitrification of the samples consisting of multiple nucleations of small grains or decomposition of the unstable phase upon annealing [71]. In the latter case, the recrystallization process can involve the dissolution of the unstable nanocrystallites, with the formation and growing of more stable nanocrystals [71,72]. The significant variation in the value of the nanocrystalline grain size can strongly affect the magnetization behavior of the NiMnGa samples, which will be explained in the following sections. While the primary trend observed from calculations, particularly through the application of the Debye–Scherrer equation, indicates significant grain growth, it is also important to acknowledge that other factors, such as microstrain within the crystallites, can influence the peak profiles and broadening observed in the XRD patterns.

3.2. Magnetic Properties and Martensitic Transformation Behavior

Presented in Figure 4 are the thermomagnetic characterization data collected under a low magnetic field of 50 Oe, spanning temperatures from 400 K to 5 K. The as-prepared sample's ZFC, FC, and FH curves exhibit significant noise due to the high coercivity value (H_c ranging from 3150 Oe to 420 Oe). However, a rather weak martensitic phase transition is observed in the FC and FH curves measured with a high applied magnetic field exceeding 3 kOe. This behavior is similar to that reported for as-prepared NiMnGa microwire with a small aspect ratio [19] and NiMnGa microwires annealed at an elevated temperature [52].

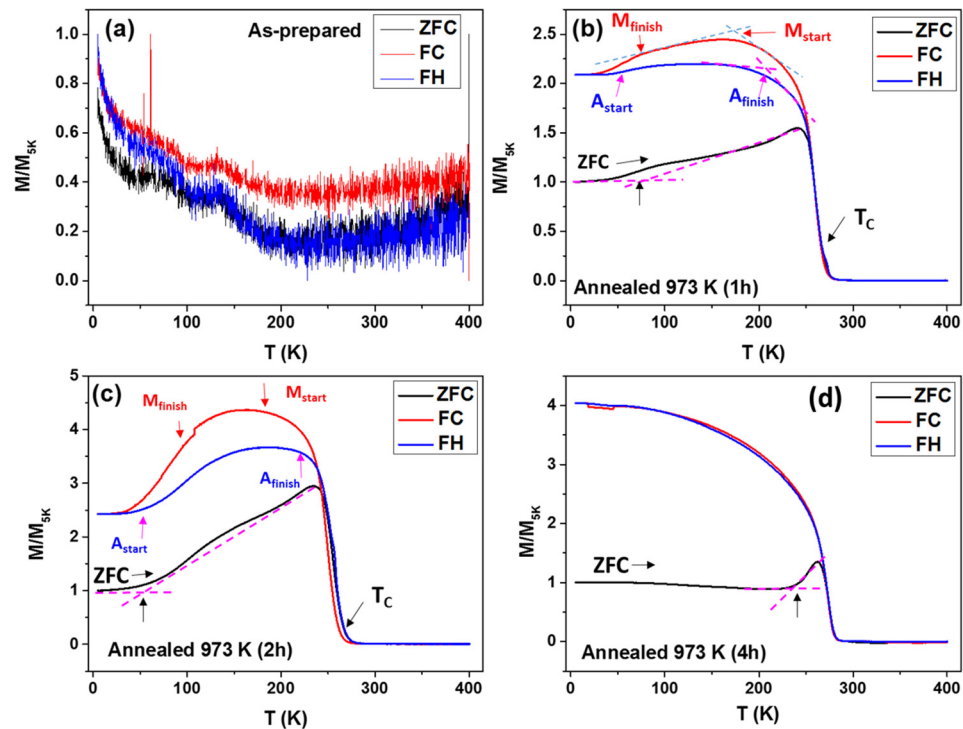


Figure 4. Zero-field-cooled (ZFC), field-cooled (FC), and field-heated (FH) magnetization curves measured under an applied field of 50 Oe. (a) As-prepared NiMnGa glass-coated microwires; (b–d) samples annealed at 973 K for (b) 1 h, (c) 2 h, and (d) 4 h, respectively.

For the samples annealed for 1 h and 2 h, the ZFC curve shows a steady increase in magnetization as the temperature rises. The changes in slope observed at 90 K and 50 K, respectively, can be attributed to the beginning of the martensite-to-austenite phase transformation (A_{start}). The kinks in the ZFC curves at 233 K (Figure 4b) and 220 K (Figure 4c) correspond to the completion of austenite formation (A_{finish}). For the samples annealed for 1 h and 2 h, above their respective structural transition temperatures (245 K and 235 K), a Hopkinson peak is observed. This is followed by the Curie temperature (T_c), measured at 282 K for the 1 h annealed sample and 273 K for the 2 h sample. In the FC curves of the annealed samples, a small kink is visible at 180 K (1 h) and 171 K (2 h), corresponding to the Hopkinson maximum. Magnetization then increases further up to 166 K (1 h) and 152 K (2 h), indicating the martensitic start temperature (M_{start}). The drop in magnetization at 85 K (1 h) and 77 K (2 h) signifies the completion of the martensitic transformation (M_{finish}). Additionally, the temperature hysteresis observed between the FC and FH curves for the 1 h and 2 h annealed samples is characteristic of the martensitic transformation (MT). Interestingly, the sample annealed for 4 h does not exhibit this temperature hysteresis behavior (see Figure 4d).

As Figure 4 demonstrates, the annealing conditions have a significant impact on the magnetic properties and martensitic transformation (MT) behavior of the studied NiMnGa glass-coated microwires. Notably, the as-prepared sample exhibits a ferromagnetic ordering with a Curie temperature (T_c) near room temperature. Annealing effectively shifts the T_c below room temperature and enhances the MT response. Conversely, the as-prepared sample shows negligible MT behavior with a T_c exceeding room temperature. Our previous studies on NiMnGa glass-coated microwires with larger diameters compared to those in the present study revealed that annealing shifted the T_c above room temperature, and the as-prepared samples displayed rather soft magnetic properties with minimal MT at low fields.

The martensitic transformation observed in samples annealed for 1–2 h represents a diffusionless structural transition from a high-symmetry cubic austenite phase to a low-symmetry martensite phase. This first-order transformation exhibits characteristic temperature hysteresis, as clearly evidenced by the divergence between heating and cooling curves in the $M/M_{5K}(T)$ dependencies (Figure 4b,c). Such hysteretic behavior results in distinct temperature-dependent phase fraction evolution during the heating and cooling cycles. The transformation temperatures (T_c and T_M) are fundamentally governed by the alloy's chemical composition, particularly the valence electron concentration (e/a) ratio [71–73]. This explains the remarkable sensitivity of both magnetic and MT properties to subtle variations in microstructure and stoichiometry, as demonstrated by the 4 h annealed sample where no significant MT occurs (Figure 4d). The absence of transformation in this sample underscores how minor compositional or structural modifications can dramatically alter the material's phase transition behavior.

Additionally, internal stresses arising during the preparation of glass-coated microwires using rapid melt quenching of NiMnGa microwire inside the glass-coating with substantially different thermal expansion coefficients can affect the microstructure and hence the magnetic properties of Heusler-type microwires or thin films [7,60,74]. Accordingly, internal stress relaxation through annealing can substantially affect the magnetic properties of the studied Heusler-type NiMnGa microwire.

3.3. Hysteresis Loops

Figures 5 and 6 present the hysteresis loops (represented as normalized magnetization, M/M_{5K} , versus magnetic field, H) for NiMnGa microwires with a glass coating. The measurements were performed at various temperatures ranging from 300 K (room temperature) to 5 K for both the as-prepared sample and those annealed for different durations. Intriguingly, the as-prepared sample exhibits unexpectedly high coercivity and remanence from 300 K to 200 K (see Figure 5), suggesting a magnetically hard behavior. In contrast, the hysteresis loops measured at the lowest temperature (5 K) for the annealed samples reveal a very soft ferromagnetic character (see Figure 6). Additionally, the hysteresis loops obtained at 300 K for the annealed samples exhibit pronounced paramagnetic behavior, appearing nearly linear with minimal remanence and coercivity (see Figure 5). These findings imply a significant relationship between the annealing parameters and the magnetic characteristics of the NiMnGa glass-coated microwires. This connection is further underscored by the evident fluctuations in the Curie temperature (T_c). Our data show that the T_c for the as-prepared sample exceeds room temperature, whereas the T_c for the annealed samples (irrespective of annealing time) is observed to be below room temperature. It is widely recognized that the Curie temperature in NiMnGa alloys is acutely responsive to elements like chemical composition, microstructure, fabrication techniques, and thermal treatment [7,52,70,75–77]. Specifically, the documented range for the Curie temperature within this alloy system spans from 160 K to 360 K. This sensitivity suggests that the microstructure is a critical determinant of both the T_c value and, as will be explored subsequently, the comprehensive magnetic behavior of the NiMnGa glass-coated microwires.

The $H_c(T)$ (temperature-dependent coercivity) and $M_r(T)$ (temperature-dependent remanence) dependencies for the as-prepared and annealed samples are provided in Figures 7 and 8. The as-prepared sample shows the highest H_c -values for all the measured temperatures, where the highest H_c -value ($H_c \approx 3150$ Oe) is observed at $T = 200$ K and the lowest $H_c \approx 420$ Oe is observed at $T = 5$ K (see Figure 7a). The H_c -value for the as-prepared sample is 53 times higher than the H_c for the annealed samples for 1 h and 2 h and 13 times higher than for the annealed sample for 4 h measured at the same temperature ($T = 200$ K). In addition, the $H_c(T)$ dependence is substantially affected by the annealing temperature

and duration. For all the NiMnGa-based glass-coated microwires, i.e., as-prepared and annealed samples, the $H_c(T)$ follows a monotonic increasing in its value by decreasing the temperature from 300 K to 200 K. Then, a sharp drop in the H_c -value with the T decreasing below 200 K is seen in the as-prepared sample (see Figure 7a). Meanwhile, a monotonic increasing in H_c values by decreasing the temperature is observed in all the annealed samples (see Figure 7b–d).

Regarding the $M_r(T)$ dependencies, the as-prepared sample shows more complex $M_r(T)$ dependencies compared to the annealed samples. Two flip points at $T = 250$ K and 50 K are observed, where the $M_r(T)$ dependencies change (see Figure 8a). For the annealed samples, similar $M_r(T)$ dependencies are observed for the samples annealed for 1 h and 4 h, where monotonic increasing in the M_r -values by decreasing the temperature from 300 K to 5 K is recorded (see Figure 8b,d). For the sample annealed for 2 h, two flip points are seen at $T = 150$ K and 20 K, where the $M_r(T)$ dependencies change tendencies. The M_r and $H_c(T)$ dependencies reveal the strong effect of the annealing condition on the magnetic behavior of the studied NiMnGa-based glass-coated microwires.

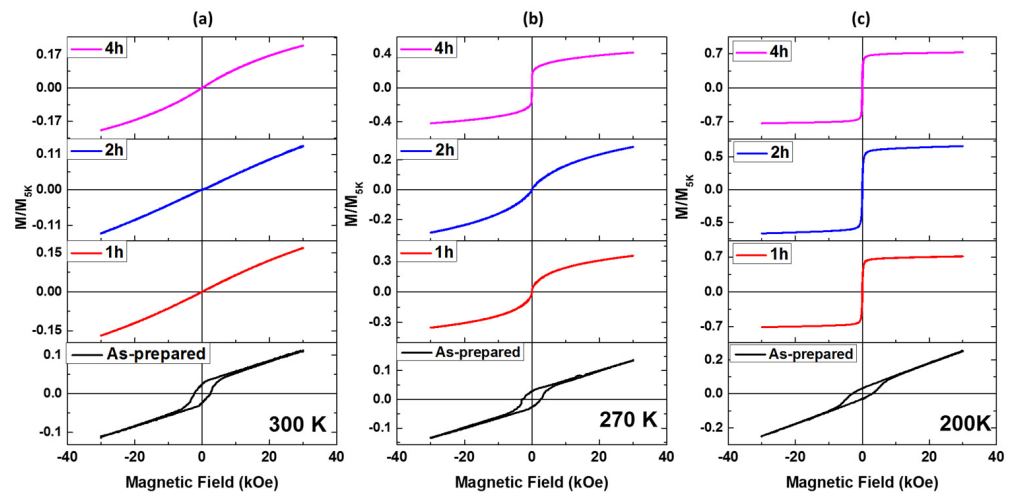


Figure 5. Hysteresis loops of as-prepared and annealed NiMnGa-based glass-coated microwires at 973 K for 1 h, 2 h, and 4 h measured at different temperatures: (a) 300 K, (b) 270 K, and (c) 200 K. M_{5K} is defined as “the magnetic moment recorded at 5 K”.

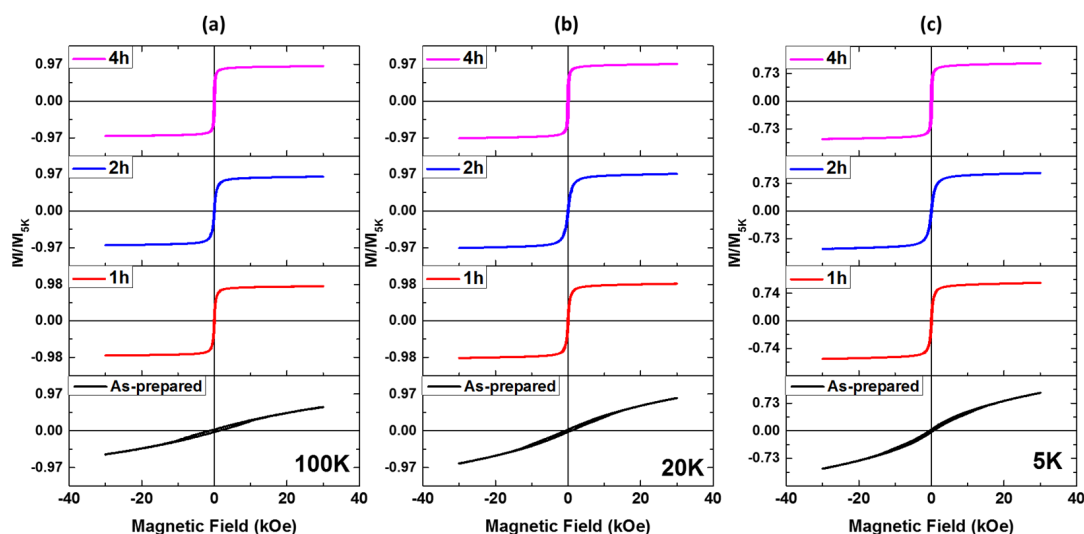


Figure 6. Hysteresis loops of as-prepared and annealed NiMnGa-based glass-coated microwires at 973 K for 1 h, 2 h, and 4 h measured at different temperatures: (a) 100 K, (b) 20 K, and (c) 5 K. M_{5K} is defined as “the magnetic moment recorded at 5 K”.

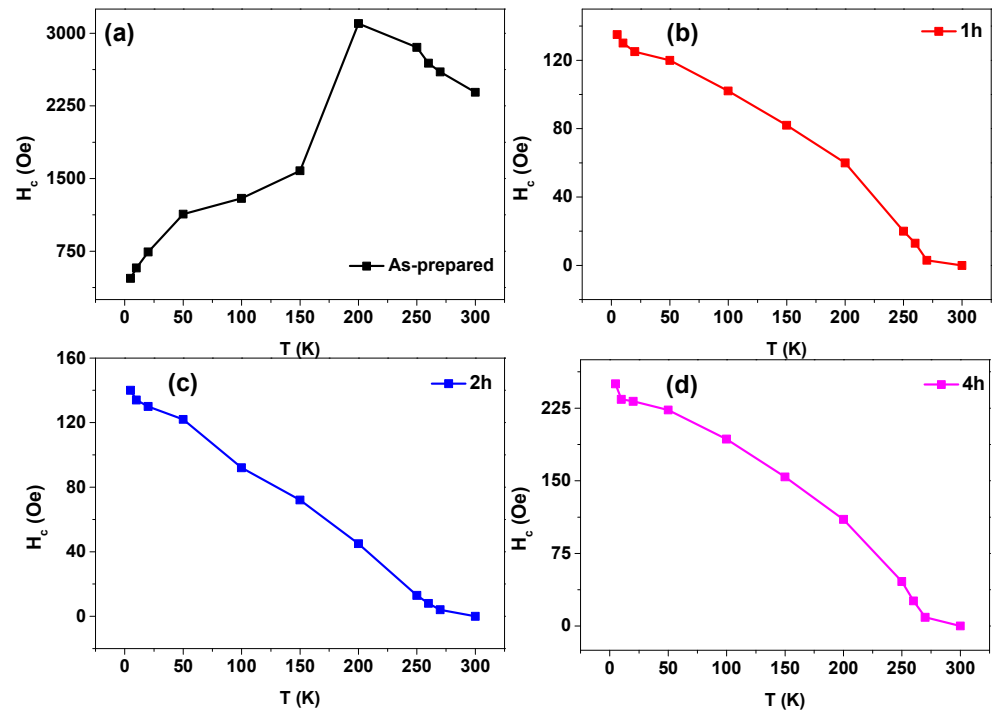


Figure 7. Temperature dependence of in-plane coercivity for as-prepared (a) and annealed at 973 K for (b) 1 h, (c) 2 h and (d) 4 h NiMnGa-based glass-coated microwires. Solid lines serve as visual guides.

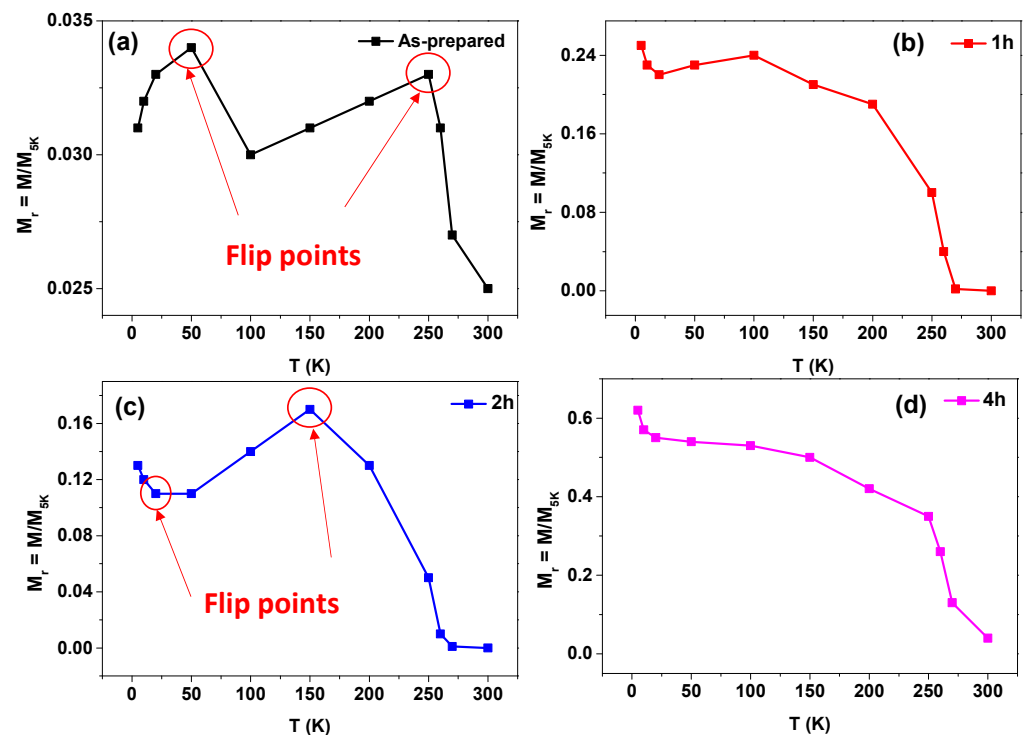


Figure 8. Illustration of how the in-plane remanence (M_r) varies with temperature for NiMnGa-based glass-coated microwires in their as-prepared state (a) and after annealing at 973 K for durations of (b) 1 h, (c) 2 h, and (d) 4 h. Lines are provided to help guide the viewer's eye along the data.

Figure 9 presents the temperature dependence of the spontaneous exchange bias field (H_{EB}) for both the as-prepared and annealed samples. The observation of H_{EB} is frequently reported in NiMnGa alloys and is attributed to the coexistence of antiferromagnetic and ferromagnetic phases at various temperature ranges [19,70]. Notably, our study demon-

strates spontaneous exchange bias (observed even under zero-field-cooled, ZFC, protocol). The H_{EB} -values are comparable to those found in other studies of NiMnGa microwires, but such exchange bias was observed in field-cooled (FC) NiMnGa microwires [70].

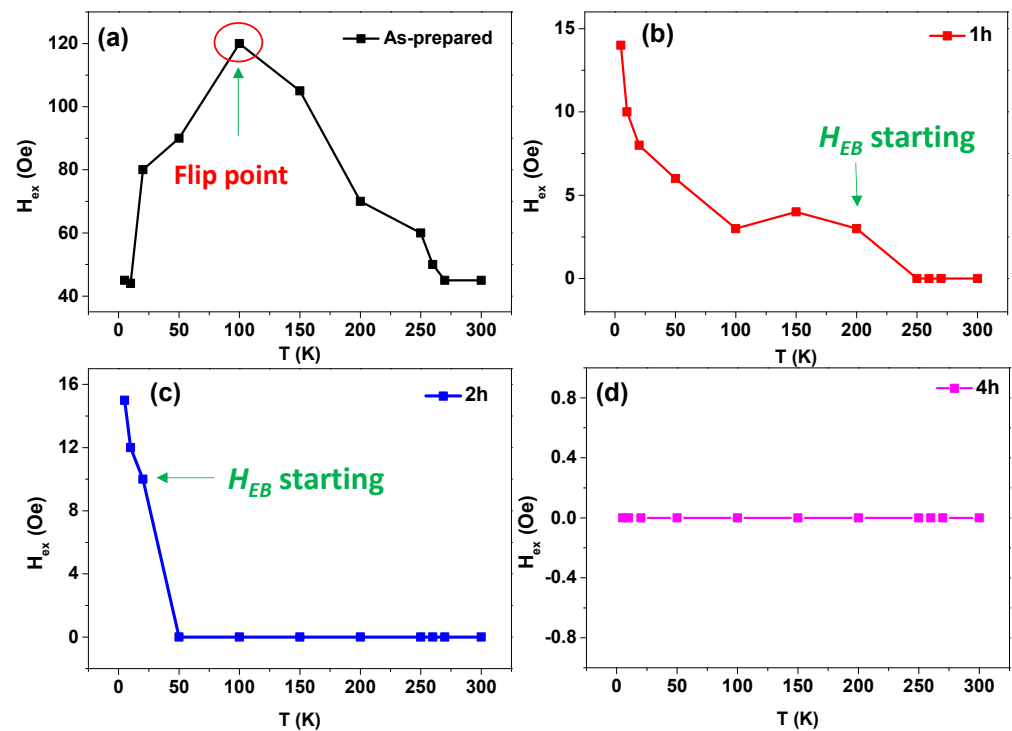


Figure 9. Temperature dependence of the spontaneous exchange bias for as-prepared (a) and annealed NiMnGa-based glass-coated microwires at 973 K for (b) 1 h, (c) 2 h, and (d) 4 h (lines for eye guide).

As illustrated in Figure 9, the as-prepared sample exhibits the highest H_{EB} -value, compared to the annealed samples. Additionally, the H_{EB} exhibits a temperature dependence with a distinct maximum around 100 K. For the annealed samples, the onset of spontaneous exchange bias appears below room temperature. Specifically, H_{EB} starts to appear at 200 K and 20 K in the samples annealed for 1 h and 2 h, respectively. Interestingly, the 4 h annealed sample shows no observable spontaneous exchange bias. The H_{EB} -value for the as-prepared sample is at least 40 times higher than that observed in the samples annealed for 1 h and 2 h. As shown in Figure 9b,c, the $H_{EB}(T)$ dependence exhibits a monotonic increase for the 1 h and 2 h annealed samples, with H_{EB} increasing as the temperature decreases from 200 K to 5 K and 20 K to 5 K, respectively.

Motivated by these remarkable observations of spontaneous exchange bias, we plan to conduct further studies focusing on the conventional exchange bias behavior of these samples in the near future.

4. Conclusions

This study demonstrates the successful fabrication of ultrathin ($\approx 5 \mu\text{m}$), long (up to several meters), and flexible NiMnGa-based glass-coated microwires. The annealing conditions were found to critically influence the magnetic properties of the microwires, including hysteresis loops, temperature-dependent magnetization, and Curie temperature. Post-annealing—which facilitates internal stress relaxation, disorder reduction, and recrystallization—revealed a hysteretic anomaly in the $M/M_5K(T)$ dependencies. Notably, a distinct magnetic softening appeared near 260 K in samples annealed at 973 K for 1–2 h, suggesting a first-order phase transformation.

These findings are analyzed in relation to the nanocrystalline structure of both as-prepared and annealed samples, with particular emphasis on the magnetic ordering of phases before and after annealing. The flexible glass coating not only enhances the mechanical durability of these otherwise fragile microwires but also provides electrical insulation—a key advantage for practical applications. However, the glass coating also significantly impacts the microstructure and magnetic behavior, underscoring the need for optimized annealing conditions to achieve the desired martensitic transformation.

This work highlights the delicate balance between material processing and functional performance, providing insights for the future design and optimization of Heusler-type microwires.

Author Contributions: Conceptualization, M.S. and A.Z.; methodology, M.S. and V.Z.; validation, M.S., V.Z. and A.Z.; formal analysis, M.S.; investigation, M.S. and A.Z.; resources, V.Z. and A.Z.; data curation M.S. and V.Z.; writing—original draft preparation, M.S. and A.Z.; writing—review and editing, M.S. and A.Z.; visualization, M.S. and V.Z.; supervision, A.Z.; project administration, V.Z. and A.Z.; funding acquisition, J.G., V.Z. and A.Z. All authors have read and agreed to the published version of the manuscript.

Funding: This research was funded by the Spanish MICIN (project PID2022-141373NB-I00), the EU (Horizon Europe projects “INFINITE” and “HARMONY”), and the Government of the Basque Country (Elkartek projects MOSINCO and ATLANTIS, and “Ayuda a Grupos Consolidados”, Ref.: IT1670-22).

Data Availability Statement: The data that support the findings of this study are available on request from the corresponding author.

Acknowledgments: The authors thank SGIker of UPV/EHU (Medidas Magnéticas Gipuzkoa) and European funding (ERDF and ESF) for their technical and human support. Furthermore, author MS acknowledges funding from the Spanish Ministerio de Universidades and the European Union—Next Generation EU under the Maria Zambrano contract.

Conflicts of Interest: The authors declare no conflicts of interest.

References

1. Moya, X.; Kar-Narayan, S.; Mathur, N.D. Caloric materials near ferroic phase transitions. *Nat. Mater.* **2014**, *13*, 439–450. [[CrossRef](#)] [[PubMed](#)]
2. Manosa, L.; Planes, A. Materials with giant mechanocaloric effects: Cooling by strength. *Adv. Mater.* **2017**, *29*, 1603607. [[CrossRef](#)]
3. Tavares, S.; Yang, K.; Meyers, M.A. Heusler alloys: Past, properties, new alloys, and prospects. *Prog. Mater. Sci.* **2023**, *132*, 101017. [[CrossRef](#)]
4. Guillou, F.; Porcari, G.; Yibole, H.; van Dijk, N.; Bruck, E. Taming the first-order transition in giant magnetocaloric materials. *Adv. Mater.* **2014**, *26*, 2671–2675. [[CrossRef](#)]
5. Li, D.; Li, Z.; Yang, J.; Li, Z.; Yang, B.; Yan, H.; Wang, D.; Hou, L.; Li, X.; Zhang, Y.; et al. Large elastocaloric effect driven by stress-induced two-step structural transformation in a directionally solidified Ni₅₅Mn₁₈Ga₂₇ alloy. *Scr. Mater.* **2019**, *163*, 116–120. [[CrossRef](#)]
6. Bonnot, E.; Romero, R.; Manosa, L.; Vives, E.; Planes, A. Elastocaloric effect associated with the martensitic transition in shape-memory alloys. *Phys. Rev. Lett.* **2008**, *100*, 125901. [[CrossRef](#)] [[PubMed](#)]
7. Zhukova, V.; Aliev, A.M.; Varga, R.; Aronin, A.; Abrosimova, G.; Kiselev, A.; Zhukov, A. Magnetic Properties and MCE in Heusler-Type Glass-Coated Microwires. *J. Supercond. Novel Magn.* **2013**, *26*, 1415–1419. [[CrossRef](#)]
8. Tang, X.; Feng, Y.; Wang, H.; Wang, P. Enhanced elastocaloric effect and cycle stability in B and Cu co-doping Ni-Mn-In polycrystals. *Appl. Phys. Lett.* **2019**, *114*, 033901. [[CrossRef](#)]
9. Salaheldeen, M.; Zhukova, V.; Gonzalez, J.; Zhukov, A. Anomalous magnetic behavior in MnFePSi glass-coated microwires. *J. Alloys Compd.* **2024**, *1002*, 175244. [[CrossRef](#)]
10. Neese, B.; Chu, B.; Lu, S.G.; Wang, Y.; Furman, E.; Zhang, Q.M. Large electrocaloric effect in ferroelectric polymers near room temperature. *Science* **2008**, *321*, 821–823. [[CrossRef](#)]
11. Liu, J.; Gottschall, T.; Skokov, K.P.; Moore, J.D.; Gutfleisch, O. Giant magnetocaloric effect driven by structural transitions. *Nat. Mater.* **2012**, *11*, 620–626. [[CrossRef](#)] [[PubMed](#)]

12. Chernenko, V.A.; Besseghini, S.; Hagler, M.; Mullner, P.; Ohtsuka, M.; Stortiero, F. Properties of sputter-deposited Ni-Mn-Ga thin films. *Mater. Sci. Eng. A* **2008**, *481–482*, 271–274. [[CrossRef](#)]
13. Ma, S.; Zhang, X.; Zheng, G.; Qian, M.; Geng, L. Toughening of Ni-Mn-Based Polycrystalline Ferromagnetic Shape Memory Alloys. *Materials* **2023**, *16*, 5725. [[CrossRef](#)]
14. Cong, D.Y.; Huang, L.; Hardy, V.; Bourgault, D.; Sun, X.M.; Nie, Z.H.; Wang, M.G.; Ren, Y.; Entel, P.; Wang, Y.D. Low-field-actuated giant magnetocaloric effect and excellent mechanical properties in a NiMn-based multiferroic alloy. *Acta Mater.* **2018**, *146*, 142–151. [[CrossRef](#)]
15. Hirohata, A.; Sagar, J.; Lari, L.; Fleet, L.R.; Lazarov, V.K. Heusler-alloy films for spintronic devices. *Appl. Phys. A* **2013**, *111*, 423–430. [[CrossRef](#)]
16. Wojcik, A.; Chulist, R.; Czaja, P.; Kowalczyk, M.; Zackiewicz, P.; Schell, N.; Maziarz, W. Evolution of microstructure and crystallographic texture of Ni-Mn-Ga melt-spun ribbons exhibiting 1.15% magnetic field-induced strain. *Acta Mater.* **2021**, *219*, 117237. [[CrossRef](#)]
17. Wu, Y.F.; Xuan, H.C.; Agarwal, S.; Xu, Y.K.; Zhang, T.; Feng, L.; Li, H.; Han, P.D.; Zhang, C.L.; Wang, D.; et al. Large magnetocaloric effect and magnetoresistance in Fe and Co co-doped Ni-Mn-Al Heusler alloys. *Phys. Status Solidi A*. **2018**, *215*, 1700843. [[CrossRef](#)]
18. Franco, V.; Blázquez, J.S.; Ipus, J.J.; Law, J.Y.; Moreno-Ramírez, L.M.; Conde, A. Magnetocaloric effect: From materials research to refrigeration devices. *Prog. Mater. Sci.* **2018**, *93*, 112–232.
19. Salaheldeen, M.; Zhukova, V.; Lopez Anton, R.; Zhukov, A. Dependence of Magnetic Properties of As-Prepared Nanocrystalline Ni₂MnGa Glass-Coated Microwires on the Geometrical Aspect Ratio. *Sensors* **2024**, *24*, 3692. [[CrossRef](#)]
20. Graf, T.; Parkin, S.S.P.; Felser, C. Heusler Compounds—A Material Class With Exceptional Properties. *IEEE Tran. Magn.* **2011**, *47*, 367–373. [[CrossRef](#)]
21. Otsuka, K.; Wayman, C.M. *Shape Memory Materials*; Cambridge University Press: Cambridge, UK, 1999.
22. Pushin, V.G. Alloys with a Termomechanical Memory: Structure, properties and application. *Phys. Met. Metallogr.* **2000**, *90* (Suppl. S1), S68–S95.
23. Cesare, E.; Pons, J.; Santamarta, R.; Seguí, C.; Chernenko, V.A. Ferromagnetic Shape Memory Alloys: An Overview. *Arch. Metall. Mater.* **2004**, *49*, 779–789.
24. Ilyn, M.I.; Zhukova, V.; Santos, J.D.; Sánchez, M.L.; Prida, V.M.; Hernando, B.; Larin, V.; González, J.; Tishin, A.M.; Zhukov, A. Magnetocaloric effect in nanogranular glass coated microwires. *Phys. Stat. Sol.* **2008**, *205*, 1378–1381. [[CrossRef](#)]
25. Otsuka, K.; Ren, X. Physical Metallurgy of Ti-Ni-based Shape Memory Alloys. *Prog. Mater. C.* **2005**, *50*, 511–678. [[CrossRef](#)]
26. Wilson, J.; Weselowsky, M. Shape Memory Alloys for Seismic Response Modification: A State-of-the-Art Review. *Earthq. Spectra.* **2005**, *21*, 569–601. [[CrossRef](#)]
27. Dong, J.; Cai, C.; Okeil, A. Overview of Potential and Existing Applications of Shape Memory Alloys in Bridges. *J. Bridg. Eng.* **2011**, *16*, 305–315. [[CrossRef](#)]
28. Lobodyuk, V.A.; Koval', Y.N.; Pushin, V.G. Crystal-Structural Features of Pretransition Phenomena and Thermoelastic Martensitic Transformations in Alloys of Nonferrous Metals. *Phys. Met. Metallogr.* **2011**, *111*, 165–189. [[CrossRef](#)]
29. Gomes, A.M.; Khan, M.; Stadler, S.; Ali, N.; Dubenko, I.; Takeuchi, A.Y.; Guimaraes, A.P. Magnetocaloric Properties of the Ni₂Mn_{1-x}(Cu, Co)_xGa Heusler Alloys. *J. Appl. Phys.* **2006**, *99*, 08Q106. [[CrossRef](#)]
30. Salaheldeen, M.; Wederni, A.; Ipatov, M.; Zhukova, V.; Zhukov, A. Preparation and Magneto-Structural Investigation of High Ordered (L21 Structure) Co₂MnGe Microwires. *Processes* **2023**, *11*, 1138. [[CrossRef](#)]
31. Cong, D.Y.; Xiong, W.X.; Planes, A.; Ren, Y.; Mañosa, L.; Cao, P.Y.; Nie, Z.H.; Sun, X.M.; Yang, Z.; Hong, X.F.; et al. Colossal elastocaloric effect in ferroelastic Ni-Mn-Ti alloys. *Phys. Rev. Lett.* **2019**, *122*, 255703. [[CrossRef](#)]
32. Callaway, J.D.; Hamilton, R.F.; Sehitoglu, H.; Miller, N.; Maier, H.J.; Chumlyakov, Y. Shape Memory and Martensite Deformation Response of Ni₂MnGa. *Smart Mater. Struct.* **2007**, *16*, S108–S114. [[CrossRef](#)]
33. Pons, J.; Cesari, E.; Seguí, C.; Masdeu, F.; Santamarta, R. Ferromagnetic Shape Memory Alloys: Alternatives to Ni-Mn-Ga. *Mater. Sci. Eng. A* **2008**, *481–482*, 57–65. [[CrossRef](#)]
34. de Paula, V.G.; Reis, M.S. All-d-metal full Heusler alloys: A novel class of functional materials. *Chem. Mater.* **2021**, *33*, 5483–5495. [[CrossRef](#)]
35. Wei, Z.Y.; Liu, E.K.; Chen, J.H.; Li, Y.; Liu, G.D.; Luo, H.Z.; Xi, X.K.; Zhang, H.W.; Wang, W.H.; Wu, G.H. Realization of multifunctional shape-memory ferromagnets in all-d-metal Heusler phases. *Appl. Phys. Lett.* **2015**, *107*, 022406. [[CrossRef](#)]
36. Bachagha, T.; Suñol, J. All-d-Metal Heusler Alloys: A Review. *Metals* **2023**, *13*, 111. [[CrossRef](#)]
37. Zhang, Y.; Hughes, R.A.; Britten, J.F.; Dube, P.A.; Preston, J.S.; Botton, G.A.; Niewczas, M. Magnetocaloric effect in Ni-Mn-Ga thin films under concurrent magnetostructural and curie transitions. *J. Appl. Phys.* **2011**, *110*, 013910. [[CrossRef](#)]
38. Li, Z.B.; Sánchez Llamazares, J.L.; Sánchez-Valdés, C.F.; Zhang, Y.D.; Esling, C.; Zhao, X.; Zuo, L. Microstructure and magnetocaloric effect of melt-spun Ni₅₂Mn₂₆Ga₂₂ ribbon. *Appl. Phys. Lett.* **2012**, *100*, 174102. [[CrossRef](#)]
39. Wang, J.; Jiang, C.; Techapiesanchaorenkij, R.; Bono, D.; Allen, S.M.; O'Handley, R.C. Microstructure and magnetic properties of melt spinning Ni-Mn-Ga. *Intermetallics* **2013**, *32*, 151–155. [[CrossRef](#)]

40. Zhukov, A.; Garcia, C.; Ilyn, M.; Varga, R.; del Val, J.J.; Granovsky, A.; Rodionova, V.; Ipatov, M.; Zhukova, V. Magnetic and transport properties of granular and Heusler-type glass-coated microwires. *J. Magn. Magn. Mater.* **2012**, *324*, 3558–3562. [[CrossRef](#)]
41. Qian, M.F.; Zhang, X.X.; Wei, L.S.; Martin, P.; Sun, J.F.; Geng, L.; Scott, T.B.; Peng, H.X. Tunable magnetocaloric effect in Ni-Mn-Ga microwires. *Sci. Rep.* **2018**, *8*, 16574. [[CrossRef](#)]
42. Qian, M.F.; Zhang, X.X.; Li, X.; Zhang, R.C.; Martin, P.G.; Sun, J.F.; Geng, L.; Scott, T.B.; Peng, H.X. Magnetocaloric effect in bamboo-grained Ni-Mn-Ga microwires over a wide working temperature interval. *Mater. Des.* **2020**, *190*, 108557. [[CrossRef](#)]
43. Zheng, P.; Kucza, N.J.; Patrick, C.L.; Müllner, P.; Dunand, D.C. Mechanical and magnetic behavior of oligocrystalline Ni-Mn-Ga microwires. *J. Alloys Compd.* **2015**, *624*, 226–233. [[CrossRef](#)]
44. Salaheldeen, M.; Wederni, A.; Ipatov, M.; Gonzalez, J.; Zhukova, V.; Zhukov, A. Elucidation of the strong effect of the annealing and the magnetic field on the magnetic properties of Ni₂-based Heusler microwires. *Crystals* **2022**, *12*, 1755. [[CrossRef](#)]
45. Ding, Z.; Zhu, J.; Zhang, X.; Liu, D.; Qi, Q.; Zhang, Y.; Cong, D. 14% recoverable strain in Ni_{52.87}Mn_{23.82}Ga_{23.32} microwires. *J. Appl. Phys. D* **2016**, *50*, 095303. [[CrossRef](#)]
46. Chiriac, H.; Lupu, N.; Stoian, G.; Ababei, G.; Corodeanu, S.; Óvári, T.A. Ultrathin Nanocrystalline Magnetic Wires. *Crystals* **2017**, *7*, 48. [[CrossRef](#)]
47. Cobeño, A.F.; Zhukov, A.; de Arellano-Lopez, A.R.; Elías, F.; Blanco, J.M.; Larin, V.; González, J. Physical properties of nearly zero magnetostriction Co-rich glass-coated amorphous microwires. *J. Mater. Res.* **1999**, *14*, 3775–3783. [[CrossRef](#)]
48. Zhukov, A.; Gonzalez, J.; Torcunov, A.; Pina, E.; Prieto, M.J.; Cobeño, A.F.; Blanco, J.M.; Larin, V.; Baranov, S. Ferromagnetic resonance and Structure of Fe-based Glass-coated Microwires. *J. Magn. Magn. Mater.* **1999**, *203*, 238–240. [[CrossRef](#)]
49. Zhang, Y.; Li, M.; Wang, Y.D.; Lin, J.P.; Dahmen, K.A.; Wang, Z.L.; Liaw, P.K. Superelasticity and serration behavior in small-sized NiMnGa alloys. *Adv. Eng. Mater.* **2014**, *16*, 955–960. [[CrossRef](#)]
50. Zhukov, A.; Ipatov, M.; Corte-León, P.; Gonzalez-Legarreta, L.; Blanco, J.M.; Zhukova, V. Soft Magnetic Microwires for Sensor Applications. *J. Magn. Magn. Mater.* **2020**, *498*, 166180. [[CrossRef](#)]
51. Chiriac, H.; Ovári, T.A.; Pop, G. Internal stress distribution in glass-covered amorphous magnetic wires. *Phys. Rev. B* **1995**, *52*, 10104–10113. [[CrossRef](#)]
52. Zhang, X.X.; Miao, S.P.; Sun, J.F. Magnetocaloric effect in Ni-Mn-In-Co microwires prepared by Taylor-Ulitovsky method. *Trans. Nonferrous Met. Soc. China* **2014**, *24*, 3152–3157. [[CrossRef](#)]
53. Zhukov, A.; Ipatov, M.; del Val, J.J.; Taskaev, S.; Churyukanova, M.; Zhukova, V. First-order martensitic transformation in Heusler-type glass-coated microwires. *Appl. Phys. Lett.* **2017**, *111*, 242403. [[CrossRef](#)]
54. Zhukov, A.; Ipatov, M.; del Val, J.J.; Corte-León, P.; Gonzalez, J.; Granovsky, A.; Zhukova, V. Effect of annealing on magnetic properties of Ni-Mn-Ga glass-coated microwires. *J. Mater. Res.* **2018**, *33*, 2148–2155. [[CrossRef](#)]
55. Ulitovsky, A.V.; Maianski, I.M.; Avramenco, A.I. 1960 Method of Continuous Casting of Glass Coated Microwire. USSR Patent 128427, 6 May 1960.
56. Zhukov, A.; Corte-Leon, P.; Gonzalez-Legarreta, L.; Ipatov, M.; Blanco, J.M.; Gonzalez, A.; Zhukova, V. Advanced functional magnetic microwires for technological applications. *J. Phys. D Appl. Phys.* **2022**, *55*, 253003. [[CrossRef](#)]
57. Salaheldeen, M.; Zhukova, V.; Ipatov, M.; Zhukov, A. Unveiling the Magnetic and Structural Properties of (X₂YZ; X = Co and Ni, Y = Fe and Mn, and Z = Si) Full-Heusler Alloy Microwires with Fixed Geometrical Parameters. *Crystals* **2023**, *13*, 1550. [[CrossRef](#)]
58. Baranov, S.A.; Larin, V.S.; Torcunov, A.V. Technology, Preparation and Properties of the Cast Glass-Coated Magnetic Microwires. *Crystals* **2017**, *7*, 136. [[CrossRef](#)]
59. Salaheldeen, M.; Wederni, A.; Ipatov, M.; Zhukova, V.; Zhukov, A. Carbon-Doped Co₂MnSi Heusler Alloy Microwires with Improved Thermal Characteristics of Magnetization for Multifunctional Applications. *Materials* **2003**, *16*, 5333. [[CrossRef](#)] [[PubMed](#)]
60. Chernenko, V.A.; Ohtsuka, M.; Kohl, M.; Khovailo, V.V.; Takagi, T. Transformation behavior of Ni-Mn-Ga thin films. *Smart Mater. Struct.* **2005**, *14*, S245–S252. [[CrossRef](#)]
61. Zhukov, A.; Ipatov, M.; del Val, J.J.; Zhukova, V.; Chernenko, V.A. Magnetic and structural properties of glass-coated Heusler-type microwires exhibiting martensitic transformation. *Sci. Rep.* **2018**, *8*, 621. [[CrossRef](#)]
62. Salaheldeen, M.; Garcia-Gomez, A.; Ipatov, M.; Corte-Leon, P.; Zhukova, V.; Blanco, J.M.; Zhukov, A. Fabrication and Magneto-Structural Properties of Co₂-Based Heusler Alloy Glass-Coated Microwires with High Curie Temperature. *Chemosensors* **2022**, *10*, 225. [[CrossRef](#)]
63. Salaheldeen, M.; Ipatov, M.; Corte-Leon, P.; Zhukova, V.; Zhukov, A. Effect of Annealing on the Magnetic Properties of Co₂MnSi-Based Heusler Alloy Glass-Coated Microwires. *Metals* **2023**, *13*, 412. [[CrossRef](#)]
64. Salaheldeen, M.; Wederni, A.; Ipatov, M.; Zhukova, V.; Lopez Anton, R.; Zhukov, A. Enhancing the Squareness and Bi-Phase Magnetic Switching of Co₂FeSi Microwires for Sensing Application. *Sensors* **2023**, *23*, 5109. [[CrossRef](#)]
65. Cerqueira, M.F.; Stepikhova, M.; Kozanecki, A.; Andrés, G.; Alves, E. Crystal size and crystalline volume fraction effects on the erbium emission of nc-Si:Er grown by r.f. sputtering. *J. Nanosci. Nanotechnol.* **2010**, *10*, 2663–2668. [[CrossRef](#)]

66. Salaheldeen, M.; Garcia, A.; Corte-Leon, P.; Ipatov, M.; Zhukova, V.; Zhukov, A. Unveiling the Effect of Annealing on Magnetic Properties of Nanocrystalline Half-Metallic Heusler Co_2FeSi Alloy Glass-Coated Microwires. *J. Mater. Res. Technol.* **2022**, *20*, 4161–4172. [[CrossRef](#)]
67. Cerqueira, M.F.; Andritschky, M.; Rebouta, L.; Ferreira, J.A.; da Silva, M.F. Macrocrystalline silicon thin films prepared by RF reactive magnetron sputter deposition. *Vacuum* **1995**, *46*, 1385–1390. [[CrossRef](#)]
68. Zhukova, V.; Cobeño, A.F.; Zhukov, A.; Blanco, J.M.; Larin, V.; Gonzalez, J. Coercivity of glass-coated $\text{Fe}_{73.4-x}\text{Cu}_1\text{Nb}_{3.1}\text{Si}_{13.4+x}\text{B}_{9.1}$ ($0 \leq x \leq 1.6$) microwires. *Nanostruct. Mater.* **1999**, *11*, 1319–1327. [[CrossRef](#)]
69. Greer, A.L. Crystallization of amorphous alloys. *Metall. Mater. Trans. A* **1996**, *27*, 549–555. [[CrossRef](#)]
70. Herzer, G. Grain Size Dependence of Coercivity and Permeability in Nanocrystalline Ferromagnets. *IEEE Trans. Magn.* **1990**, *26*, 1397–1402. [[CrossRef](#)]
71. Talaat, A.; Del Val, J.J.; Zhukova, V.; Ipatov, M.; Klein, P.; Varga, R.; Gonzalez, J.; Zhdanova, M.; Churyukanova, M.; Zhukov, A. Effect of annealing on magnetic properties of nanocrystalline Hitperm-type glass-coated microwires. *J. Alloys Compd.* **2016**, *660*, 297–303. [[CrossRef](#)]
72. Serebryakov, A.V. Amorphization reactions and glass to crystal transformations in metallic materials. *J. Non-Cryst. Solids* **1993**, *156–158*, 594–597. [[CrossRef](#)]
73. Zhukov, A.; Ipatov, M.; del Val, J.J.; Chernenko, V.A.; Zhukova, V. Tailoring of magnetic properties of Heusler-type glass-coated microwires by annealing. *J. Alloys Compd.* **2018**, *732*, 561–566. [[CrossRef](#)]
74. Chernenko, V.A.; L'vov, V.A.; Zagorodnyuk, S.P.; Takagi, T. Ferromagnetism of thermoelastic martensites: Theory and experiment. *Phys. Rev. B* **2003**, *67*, 064407. [[CrossRef](#)]
75. Wu, S.K.; Yang, S.T. Effect of composition on transformation temperatures of Ni-Mn-Ga shape memory alloys. *Mater. Lett.* **2003**, *57*, 4291–4296. [[CrossRef](#)]
76. Chernenko, V.A. Compositional instability of β -phase in Ni-Mn-Ga alloys. *Scr. Mater.* **1999**, *40*, 523–527. [[CrossRef](#)]
77. Besseghini, S.; Gambardella, A.; Chernenko, V.A.; Hagler, M.; Pohl, C.; Mullner, P.; Ohtsuka, M.; Doyle, S. Transformation behavior of Ni-Mn-Ga/Si(100) thin film composites with different film thicknesses. *Eur. Phys. J. Spec. Top.* **2008**, *158*, 179–185. [[CrossRef](#)]

Disclaimer/Publisher's Note: The statements, opinions and data contained in all publications are solely those of the individual author(s) and contributor(s) and not of MDPI and/or the editor(s). MDPI and/or the editor(s) disclaim responsibility for any injury to people or property resulting from any ideas, methods, instructions or products referred to in the content.